PROCEEDINGS B

royalsocietypublishing.org/journal/rspb

Research

Cite this article: Gainett G, González VL, Ballesteros JA, Setton EVW, Baker CM, Barolo Gargiulo L, Santibáñez-López CE, Coddington JA, Sharma PP. 2021 The genome of a daddy-long-legs (Opiliones) illuminates the evolution of arachnid appendages. *Proc. R. Soc. B* **288**: 20211168.
https://doi.org/10.1098/rspb.2021.1168

Received: 15 February 2021
Accepted: 14 July 2021

Subject Category:
Genetics and genomics

Subject Areas:
developmental biology, genomics, genetics

Keywords:
Hox, *Deformed*, *Sex combs reduced*, *Egfr*, Chelicerata, Arachnida

Authors for correspondence:
Guilherme Gainett
e-mail: guilherme.gainett@wisc.edu
Vanessa L. González
e-mail: gonzalezv@si.edu

†Co-first authors.

Electronic supplementary material is available online at https://doi.org/10.6084/m9.figshare.c.5534425.

THE ROYAL SOCIETY PUBLISHING

The genome of a daddy-long-legs (Opiliones) illuminates the evolution of arachnid appendages

Guilherme Gainett[1,†], Vanessa L. González[2,†], Jesús A. Ballesteros[1], Emily V. W. Setton[1], Caitlin M. Baker[1], Leonardo Barolo Gargiulo[1], Carlos E. Santibáñez-López[3], Jonathan A. Coddington[2] and Prashant P. Sharma[1]

[1]Department of Integrative Biology, University of Wisconsin-Madison, Madison, 53706 WI, USA
[2]Global Genome Initiative, Smithsonian Institution, National Museum of Natural History, 10th and Constitution, NW, Washington, DC 20560-0105, USA
[3]Department of Biological and Environmental Sciences, Western Connecticut State University, 181 White St, Danbury, CT 06810, USA

GG, 0000-0002-9040-4863; VLG, 0000-0002-1593-4469; CMB, 0000-0002-9782-4959; LBG, 0000-0001-6084-6372; CES-L, 0000-0001-6062-282X; PPS, 0000-0002-2328-9084

Chelicerate arthropods exhibit dynamic genome evolution, with ancient whole-genome duplication (WGD) events affecting several orders. Yet, genomes remain unavailable for a number of poorly studied orders, such as Opiliones (daddy-long-legs), which has hindered comparative study. We assembled the first harvestman draft genome for the species *Phalangium opilio*, which bears elongate, prehensile appendages, made possible by numerous distal articles called tarsomeres. Here, we show that the genome of *P. opilio* exhibits a single Hox cluster and no evidence of WGD. To investigate the developmental genetic basis for the quintessential trait of this group—the elongate legs—we interrogated the function of the Hox genes *Deformed* (*Dfd*) and *Sex combs reduced* (*Scr*), and a homologue of *Epidermal growth factor receptor* (*Egfr*). Knockdown of *Dfd* incurred homeotic transformation of two pairs of legs into pedipalps, with dramatic shortening of leg segments in the longest leg pair, whereas homeosis in L3 is only achieved upon double *Dfd* + *Scr* knockdown. Knockdown of *Egfr* incurred shortened appendages and the loss of tarsomeres. The similarity of *Egfr* loss-of-function phenotypic spectra in insects and this arachnid suggest that repeated cooption of EGFR signalling underlies the independent gains of supernumerary tarsomeres across the arthropod tree of life.

1. Introduction

The advent of genomic resources has revealed complex dynamics in the evolution of chelicerate genomes. A group of six terrestrial orders (Arachnopulmonata), which includes spiders, scorpions, and pseudoscorpions, exhibit an ancient shared whole-genome duplication (WGD), as evidenced by the architecture of Hox clusters, analyses of synteny, patterns of microRNA enrichment, gene expression patterns and gene tree topologies [1–6] (figure 1*a*). Separately, genomes of all four living Xiphosura (horseshoe crabs) suggest a lineage-specific twofold genome duplication in this order, with one of these duplications occurring relatively recently [7–9]. While genomes of Acariformes and Parasitiformes (mites and ticks) suggest that these two orders were not included in the genome duplication events, they often deviate from typical arthropod datasets. As examples, the acariform mite *Tetranychus urticae* exhibits extreme genome compaction (90 Mb), in tandem with the loss of many transcription factors, which has been linked to miniaturization [10]. Similarly, the genome of the parasitiform mite *Galendromus occidentalis* exhibits an atomized Hox cluster, degradation of synteny and high rates of intron gain and loss [11].

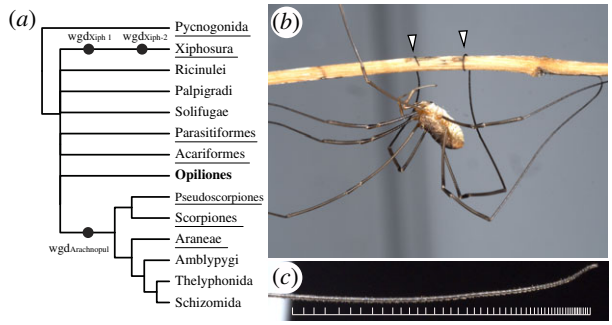

Figure 1. The significance of Opiliones in evolutionary developmental biology. (*a*) Consensus phylogeny of Chelicerata (based on [5]) and inferred WGD events in Xiphosura and Arachnopulmonata. (*b*) Adult male *P. opilio* climbing on a twig using its prehensile tarsi. (*c*) Detail of the distal subdivisions (tarsomeres) of the leg 2 tarsus. The distal terminus is to the right. White bars mark tarsomere boundaries. Photographs: Caitlin M. Baker. (Online version in colour.)

One group that may facilitate comparative genomics of Chelicerata is the arachnid order Opiliones (harvestmen) (figure 1*b*). In phylogenomic datasets, Opiliones exhibit lower evolutionary rates than Parasitiformes or Acariformes, and their placement outside of arachnopulmonates makes this group phylogenetically significant [12,13]. Developmental transcriptomes of the emerging model species *Phalangium opilio* have suggested that harvestmen do not exhibit systemic genome duplication, as evidenced by the absence of paralogy across the homeobox gene family [2,14] and gene expression patterns of genes with known paralogues in arachnopulmonates [2,6]. As a result, *P. opilio* has proven useful for the study of chelicerate developmental biology. However, the establishment of a genome for this species is a key prerequisite to validating the assumption of an unduplicated genome in this order, as well as further advancing this model system.

Beyond its use in polarizing developmental traits on phylogenetic trees, Opiliones also exhibit a suite of unique characteristics that are not found in other arthropod models. The most salient of these are the elongate walking legs in some groups (e.g. Phalangioidea, commonly termed 'daddy-long-legs'). Beyond the hypertrophied growth of certain leg segments, many daddy-long-legs exhibit subdivision of the tarsus into pseudosegments called tarsomeres, with over 100 tarsomeres in some species (figure 1*c*). Tarsomeres have evolved dynamically across the arthropod tree of life, with gains in tarsomeres across insects [15], scutigeromorph centipedes [16] and several arachnid orders. However, the tarsomeres of daddy-long-legs are sufficiently numerous that they confer prehensility to the distal leg, which is used for climbing, courtship and male–male combat (figure 1*b*). The largest number of tarsomeres in Phalangioidea typically occurs on the antenniform second leg pair, which serves as a sensory appendage [17] (figure 1*c*).

These aspects of harvestman biology position them as an opportune group for comparative study, both from the perspective of gene evolution before and after WGD, as well as understanding the genetic basis for morphological convergence (e.g. leg elongation; supernumerary tarsomeres). However, no genomes are available for any Opiliones. Moreover, the developmental genetic basis for arthropod leg elongation and tarsomere patterning is unknown outside of insects. To test the assumption that Opiliones exhibit an unduplicated genome, we generated a draft genome for *P. opilio* and leveraged this resource to investigate the genetic basis for leg patterning in this iconic arachnid group.

2. Material and methods

For brevity, detailed procedures, protocols and bioinformatic commands for the following operations are provided in the electronic supplementary material.

(a) Animal husbandry

For genome sequencing, founder population specimens of *P. opilio* were collected in Madison, WI, USA (43.074628, −89.403904), and a colony was maintained as previously described [14] (electronic supplementary material, methods).

(b) RNA sequencing

Total RNA was extracted from *ca* 250 µl of *P. opilio* embryos spanning an array of stages, reared from females captured in Weston, MA, USA. RNA extraction was performed using TRIzol reagent (ThermoFisher), following the manufacturer's protocol. mRNA purification, library construction and 2 × 150 bp sequencing on an Illumina HiSeq 2500 platform follow our previous procedures [1]. The resulting 79 472 462 paired-end reads (NCBI PRJNA690950) were combined with an older library (16 225 145 paired-end reads sequenced on an Illumina GA II; NBCI PRJNA236471) for annotation of protein-coding regions.

(c) Genome sequencing, assembly and annotation

Full-sibling inbred lines were established at a colony in Madison, WI, USA. Total genomic DNA was isolated from two specimens (fourth-generation male and sixth-generation female). Long-read sequencing was performed on a PacBio Sequel platform (Pacific Biosciences) using v. 2.1 chemistry. The single-molecule real-time (SMRT) Cells were sequenced on 16 cells with 360 min movie lengths. Short-read sequencing was performed on an Illumina HiSeq 2500 with a 350 bp insert size. Long reads were assembled using Canu v. 1.7 [18]. Contigs were processed using two rounds of scaffolding with SSPACE-LongRead v. 1.1 [19], followed by gap filling with PBJelly v. 15.8 [20] and further polishing with Pilon v. 1.23 [21]. Haplotypic duplicates were identified and removed with Purge_dups v. 1.2.3 [22]. Prior to annotation, a custom repeat library was constructed using RepeatModeler open-1.0.11 [23]. Identified repeats were masked with RepeatMasker open-4.0.6. [23]. For annotation, gene predictions generated with BRAKER2 v. 2.1.5 [24] used previously generated RNA-Seq reads from developmental transcriptomes (NCBI PRJNA236471; PRJNA690950; [12]). A genome browser was generated using MakeHub [25].

(d) Orthology inference, phylogenetic analysis and discovery of microRNAs

Homologues of *Egfr* were identified with tBLASTn [26], using query protein sequences of arthropod species for which *Egfr* expression has been previously studied. Sequence accession data are provided in the electronic supplementary material, table S1 and methods). An initial BLAST search for miRNA families in the genome of *P. opilio* and seven other chelicerates (electronic supplementary material, table S2) used as queries the miRNAs previously reported from the spider *Parasteatoda tepidariorum*, the tick *Ixodes scapularis* and the mite *T. urticae* [3,5]. To recover unique putative harvestmen miRNAs, we conducted a second search using miRNA families not known in spiders, ticks or mites, but which were shared by at least three mandibulate outgroups.

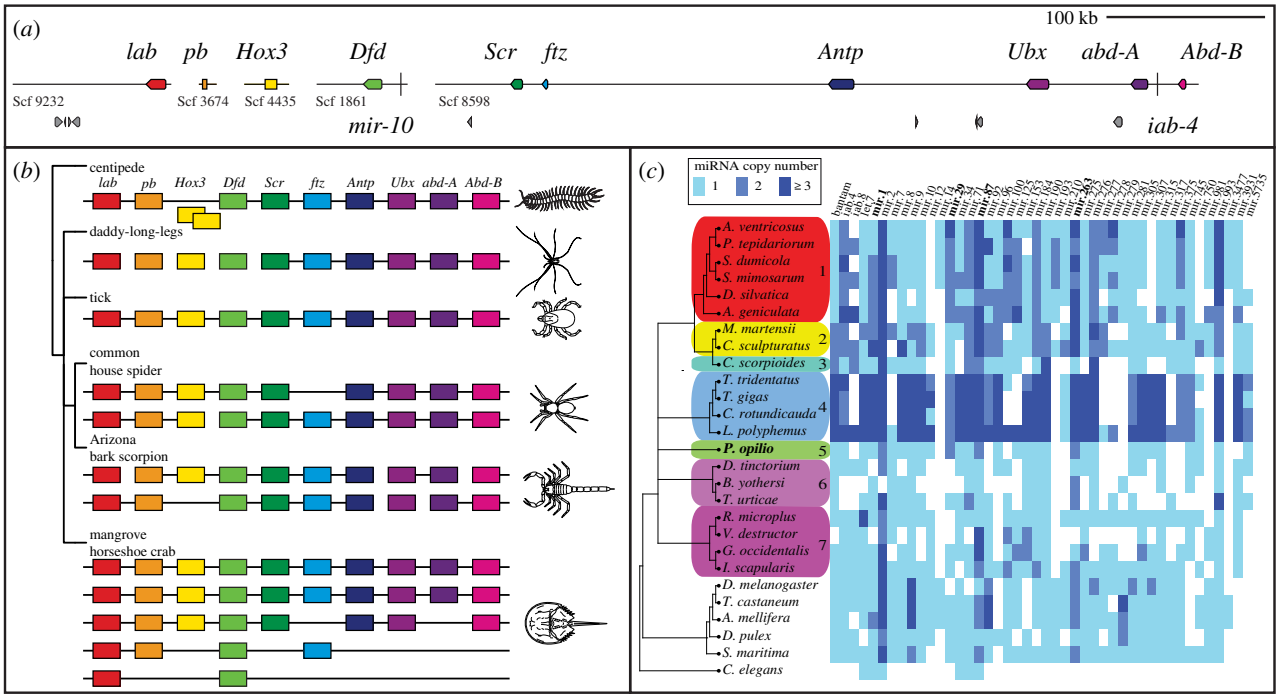

Figure 2. Hox genes and microRNAs support an unduplicated genome in the daddy-long-legs *P. opilio*. (*a*) Hox gene-containing scaffolds to scale. miRNAs *mir-10* and *iab-4* are represented by vertical bars. Hox genes are depicted in coloured boxes, and other predicted genes in grey boxes. (*b*) Hox clusters in selected arthropod genomes (after [5,31]). (*c*) Comparative analysis of miRNA families and orthologue copy numbers in *P. opilio* and other chelicerates supports retention of single copies of several families in harvestmen, in contrast to duplication found in arachnopulmonates. Columns correspond to individual miRNA families, with colours representing a different number of paralogues. miRNAs in bold are duplicated in *P. opilio* and most other chelicerates. 1: Araneae; 2: Scorpiones; 3: Pseudoscorpiones; 4: Xiphosura; 5: Opiliones; 6: Acariformes; 7: Parasitiformes. (Online version in colour.)

(e) Cloning, *in situ* hybridization and double-stranded RNA microinjection

Cloning of gene fragments, *in situ* hybridization and embryonic microinjections with dsRNA followed our previous procedures [14,27] (electronic supplementary material, tables S3 and S4). Protocols for fluorescent gene expression assays using hybridization chain reaction (HCR) followed Bruce *et al.* [28]. For harvestman RNAi experiments, approximately two-thirds of each egg clutch was injected with dsRNA and the remaining third with water (negative control). Details of the phenotype scoring strategy are provided in the electronic supplementary material.

3. Results

(a) *Phalangium opilio* draft genome assembly

The draft assembly of the *P. opilio* genome comprises 580.4 Mbp (37.5% GC content) in 5137 scaffolds (N50: 211 089) and 8349 contigs (N50: 127 429; electronic supplementary material, figure S1 and table S5). The predicted genome repetitiveness is 54.4% and estimated heterozygosity is 1.24%. The number of predicted genes after filtering steps is 20 315, which was further refined with a 98% similarity threshold and manual curation to a final gene set of 18 036. This is comparable to predicted gene sets for the tick *I. scapularis* (20 486) and the mite *T. urticae* (18 414) [10,29]. An assessment using the arthropod set of benchmarking universal single-copy orthologues (BUSCOs) [30] indicates 95.1% completeness (electronic supplementary material, figure S1 and table S5). Contamination assessment based on sequence coverage and GC content supports a relatively contamination-free assembly. The detailed description of the genome is provided in the electronic supplementary material, figures S1–S3.

(b) The genome of *Phalangium opilio* reveals the absence of Arachnopulmonata-specific whole-genome duplications

To assess whether *P. opilio* exhibits ancient WGD, we first examined the architecture of Hox clusters in this species. We discovered one 480 kb scaffold that bore six Hox genes, with the remaining four Hox genes occurring on individual scaffolds (figure 2*a*,*b*). In addition to the small size, these scaffolds contained very few or no adjacent genes, suggesting that the position of these four Hox genes outside of the main cluster is an artefact of fragmentary assembly. On the larger 480 kb scaffold, microRNAs *mir-10* and *iab-4* were located adjacent to *Dfd* and *abdA*, respectively, which reflect conserved positions with respect to other arthropods [32] (figure 2*a*). The complete peptide sequences of all 10 Hox genes corresponded to previous partial sequences predicted from developmental transcriptomes [14].

We separately examined the genome for evidence of duplicates in genes with known arachnopulmonate-specific paralogues and spatio-temporal subdivisions of expression patterns, focusing on four leg patterning genes (*dachshund*, *homothorax*, *extradenticle* and *spineless* [4,6,33]) and three retinal determination network genes (*sine oculis*, *Optix* and *orthodenticle* [34–36]). These genes all occurred as single-copy in the harvestman genome (electronic supplementary material, table S6).

We next examined the distribution of families of microRNAs (miRNAs), noncoding RNAs with important regulatory roles in animals. miRNAs have been shown to exhibit the signature of genome duplication in both Arachnopulmonata and Xiphosura [3,5]. Thirty conserved miRNA families were identified in the *P. opilio* genome (figure 2*c*).

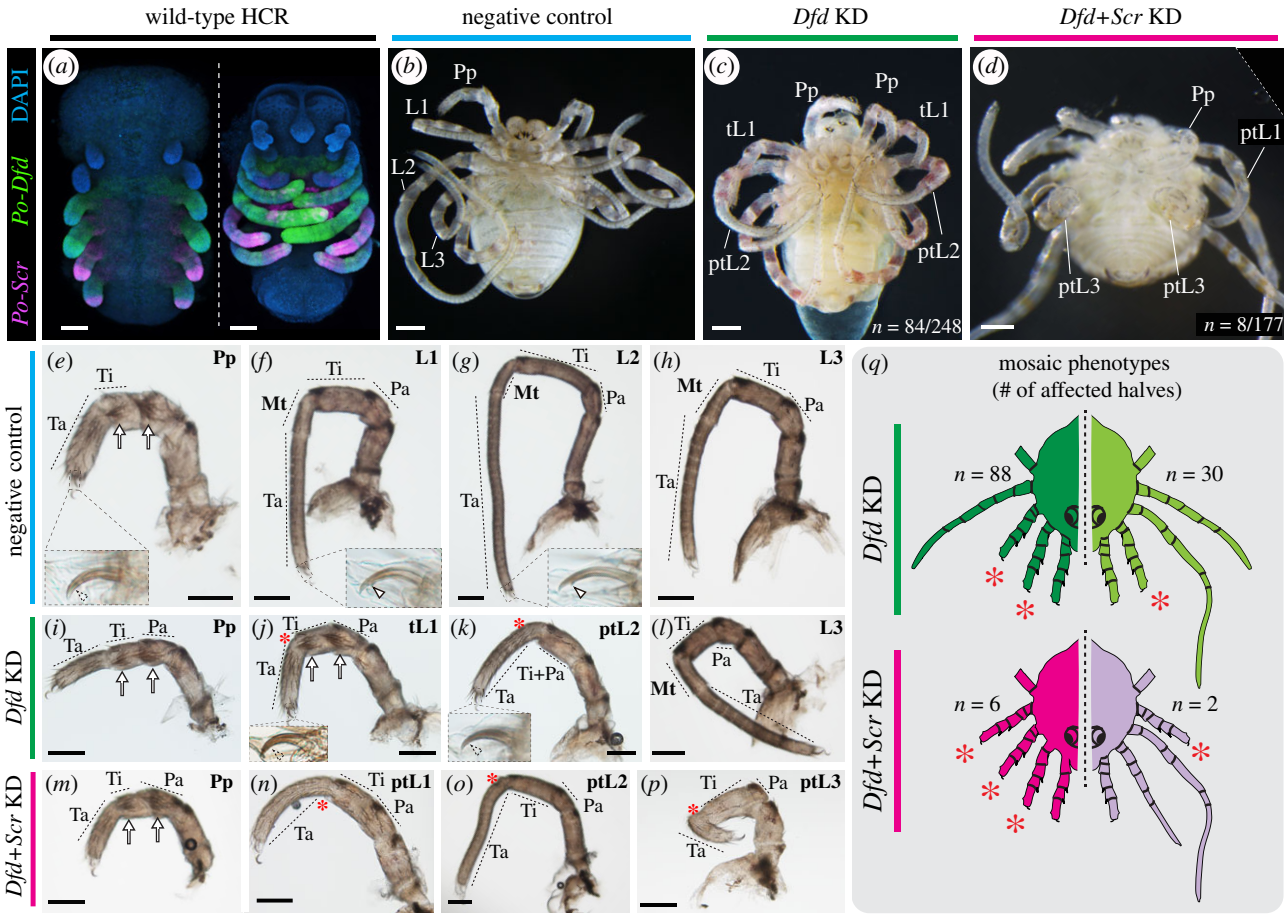

Figure 3. The single-copy orthologue of *Deformed* (*Dfd*) and *Sex combs reduced* (*Scr*) in *P. opilio* are necessary for the appendage identity of three body segments. (*a*) Wild-type HCR expression patterns of *Dfd* (green) and *Scr* (magenta) homologues in stage 11 and 15 embryos. (*c*) Wild-type (negative control) hatchling of *P. opilio*. (*c*) *P. opilio* hatchling from *Po-Dfd* RNAi treatment. (*d*) *P. opilio* hatchling from *Po-Dfd* + *Scr* RNAi treatment. (*e–h*) Appendage mounts of wild-type *P. opilio* hatchlings in lateral view. Insets: tarsal claws. (*i–l*) Appendage mounts of *Po-Dfd* RNAi hatchlings in lateral view. (*m–p*) Appendage mounts of *Po-Dfd* + *Scr* RNAi hatchlings in lateral view. (*q*) Schematic depiction of the mosaicism observed in hatchlings of *Po-Dfd* RNAi (*Dfd* KD) and *Po-Dfd* + *Scr* RNAi (*Dfd* + *Scr* KD) and distribution of phenotypic classes. Lighter colours indicate weaker penetrance. Only the two most frequent homeotic conditions are depicted (see electronic supplementary material, figure S5). Asterisk, reduced metatarsus; arrow, setal spurs; arrowhead, claw tooth; L1–L3: leg 1–3; tL1, fully transformed leg 1; ptL1–3: partially transformed legs 1–3; Mt, metatarsus; Pa, patella; Pp, pedipalp; Ta, tarsus; Ti; tibia. Scale bars: 100 µm. (Online version in colour.)

Among them, only families mir-2, mir-29, mir-87 and mir-263 had two homologues in Opiliones (figure 2*c*). These microRNAs, with the exception of mir-29, are also duplicated in most other chelicerates and outgroup arthropods, (electronic supplementary material, table S2), suggesting the origin of paralogues at the arthropod common ancestor (figure 2*c*). The presence of duplicated mir-29 in harvestmen, horseshoe crabs and a subset of Arachnopulmonata suggests separate independent duplication events in these lineages, although this parsimonious inference is contingent upon the resolution of the position of these groups in arachnid phylogeny. In sum, we found no evidence of miRNA duplications in the harvestman genome that were exclusively shared either with Arachnopulmonata or Xiphosura.

(c) *Deformed* and *Sex combs reduced* are necessary for leg fate specification in *Phalangium opilio*

Deformed homologues of arachnids are typically expressed in the four leg-bearing segments (L1–L4), whereas *Sex combs reduced* is expressed from L2 segment onwards (figure 3*a*; electronic supplementary material, figure S4) [4,14,37]. In the spider *P. tepidariorum* (a member of Arachnopulmonata), the two *Dfd* paralogues have divergent expression patterns; only *Ptep-DfdA* is expressed in the legs and expression levels are uniform across L1–L4 [4]. Knockdown of *Ptep-DfdA* results in homeotic L1-to-pedipalp transformation [38]. No functional data exist for any single-copy homologue of *Dfd* in Arachnida, and no functional data exist for *Scr* in Arachnida altogether. Intriguingly, *Po-Dfd* is also expressed in L1–L4, but much more strongly in L2 (the longest leg pair) than the other three leg pairs, particularly during leg elongation [14]. *Scr* is expressed in L3 and L4, but its expression is much stronger in L3 [14].

We first investigated the function of *Dfd* (*Po-Dfd*) through embryonic RNAi, via microinjection of double-stranded RNA (dsRNA) (electronic supplementary material, figure S5). Upon completion of embryogenesis, 33% ($n = 84/248$) of RNAi hatchlings exhibited leg-to-pedipalp homeosis affecting L1 and L2 (figure 3*b,c*; electronic supplementary material, figure S5). Complete leg-to-pedipalp homeotic transformation (figure 3*c,j*), only observed in L1, was evidenced by the loss of the metatarsus (segment specific to arachnid leg; absent in pedipalp), the presence of pedipalp-specific setal spurs, the loss of the leg-specific tooth of the distal claw (figure 3*e,f,i,j*) and the undivided tarsus. Partial transformation was evidenced by a defective or absent metatarsus (figure 3*g–k*). Strongly affected L2 also exhibited a

fusion of tibia and patella segments (figure 3*k*). Importantly, L3 and L4 were unaffected (figure 3*h*,*l*). The majority ($n = 73/84$) of *Po-Dfd* knockdown phenotypes exhibited mosaicism, with one side of the body more strongly affected (bilateral mosaics), so we further classified homeotic individuals in mosaic classes. This tabulation considered whether a given half presented no homeosis (wild-type), homeosis in both L1 and L2, homeosis in L1 only, or in L2 only (electronic supplementary material, figure S5). This analysis revealed that the most frequent homeotic conditions were having both legs affected (88/168 halves), followed by L1 only (30/168 halves) and L2 only (2/168 halves) (figure 3*q*; electronic supplementary material, figure S5). In halves with both legs affected, L1 was always more strongly transformed than L2. Notably, knockdown of *Po-Dfd* resulted in dramatic shortening of the transformed appendages, and particularly for transformed L2 (compare figure 3*g*,*k*). Reduced *Po-Dfd* expression was observed overall in embryos injected with *Po-Dfd* dsRNA and correlated with the side presenting homeotic transformation in mosaic embryos (electronic supplementary material, figure S6).

Next, to investigate a possible role of *Scr* in the identity of L3 and L4, we performed RNAi against *Po-Scr*. Despite verifiable decreased expression (electronic supplementary material, figure S6), we detected no phenotypic effects on dsRNA-injected embryos (five clutches, $n = 540$ embryos), suggesting that *Scr* may exhibit functional redundancy in arachnids. We therefore performed a double knockdown of *Po-Dfd* and *Po-Scr*. Mortality was high (153/176), but double RNAi resulted in partial leg-to-pedipalp transformation affecting L1, L2 and L3 ($n = 8/176$) (figure 3*d*, *m*–*q*; electronic supplementary material, figure S5).

Taken together, these results suggest that *Po-Dfd* is necessary for conferring leg identity of the L1 and L2 segments, and that both *Dfd* and *Scr* are necessary for the identity of the L3 segment.

(d) Epidermal growth factor receptor is necessary for distal leg patterning in the daddy-long-legs

A notable component of leg morphology in daddy-long-legs is the repeated subdivision of the tarsus, the distalmost leg segment. In insects, EGFR signalling is involved in tarsal fate specification [39–41], but it is unknown if this signalling pathway is necessary for leg patterning in chelicerates (figure 4*a*). Upon surveying the *P. opilio* genome, we discovered two *Egfr* paralogues in the harvestman (electronic supplementary material, figure S7). One of these, *Po-EgfrB*, lacks the transmembrane and intracellular domains seen in other *Egfr* homologues (electronic supplementary material, figure S8). A 3′ UTR for *Po-EgfrB* was assembled in both embryonic transcriptomes and corroborated by the genome assembly, disfavouring fragmentary assembly as a possible explanation for missing domains. We therefore focused on *Po-EgfrA*, the paralogue containing all known *Egfr* functional domains.

In early limb bud stage, *Po-EgfrA* is expressed in a strong circular domain around the stomodeum, in a strong ring at the base of each appendage and in a weak stripe along the ventral midline (figure 4*b*; electronic supplementary material, figure S9). In later stages, additional expression domains occur in the developing eye field, in a strong domain in the medial bridge of the developing brain, and in rings at the boundaries of the segments (podomeres) of the developing appendages (figure 4*c*,*d*; electronic supplementary material, figure S9). To investigate EGFR signalling further, we surveyed the expression of a homologue of *pointed*, an ETS transcription factor that acts as an EGFR signal effector [42]. In early limb bud stages, the single-copy *Po-pnt* is expressed in the ventral ectoderm and the distal tip of the appendages (figure 4*e*; electronic supplementary material figure S9). Similar to the beetle *T. castaneum* [43], in later stages, *Po-pnt* is also expressed in the head lobes, and groups of cells in the appendages, particularly in the distal region, forming rings (figure 4*f*,*g*; electronic supplementary material, figure S9).

RNAi against *EgfrA* resulted in 39.6% ($n = 36/91$) of hatchlings exhibiting segmentation and appendage defects (figure 4*h*–*t*; electronic supplementary material, figure S10); all affected embryos were bilateral mosaics (figure 4*i*,*j*) and defects correlated with reduced *Po-EgfrA* expression in embryos (electronic supplementary material, figure S11). *Po-EgfrA* dsRNA-injected hatchlings showed defects of antero-posterior (body) segmentation, with dorsal tissue fusion on the side of the body affected ($n = 29/36$), correlating with a characteristic curved shape of the body of mosaic individuals (figure 4*i*). Defects of the eyes ($n = 25/36$) ranged from a small reduction in size to complete absence (figure 4*j*).

The appendages exhibited an array of defects in terminal structures (figure 4*k*–*t*). The chelicera showed the reduction of the fixed finger, movable finger or both ($n = 11/36$) (figure 4*o*); the pedipalp showed a reduced claw ($n = 19/36$) (figure 4*p*); and, in the case of all legs, the claw and tarsomeres were reduced ($n = 26/36$) (figure 4*q*,*r*). Most notably, a subset of weakly affected individuals ($n = 10$) showed a condition in which the distalmost tarsomeres were fused and the claw was missing, or just the claw was missing (figure 4*t*). Segmental fusions in limbs occurred in a subset of hatchlings ($n = 14/36$) (figure 4*q*). The proximal segment of the appendages (coxa) showed defects ranging from reduction in size to complete proximal fusion of adjacent appendage coxae ($n = 34/36$) (figure 4*s*), which correlated with the strong ring of expression at the base of all appendages.

These results are broadly consistent with expression and functional data available for *Egfr* homologues in insect models [43–46]. The loss-of-function phenotypic spectrum in *P. opilio* suggests that *EgfrA* may underpin both leg elongation and tarsomere morphogenesis in daddy-long-legs.

4. Discussion

(a) Genomics and Hox-logic in a phylogenetically significant arachnid model

Spatio-temporal subdivision of expression domains of duplicated developmental patterning genes are systemic in Arachnopulmonata, as established by gene expression surveys in model spiders, scorpions and whip spiders [1,2,4,47]. This phenomenon makes arachnopulmonates an ideal taxon for investigating the role of gene duplication in generating body plan disparity. Identifying subfunctionalization or neofunctionalization of duplicates requires a clear inference of the ancestral single-copy homologue's expression pattern and function. In this regard, *P. opilio* has played a central role in polarizing developmental phenomena, given its phylogenetic position, low evolutionary rate and tractability in the laboratory [2,6,48].

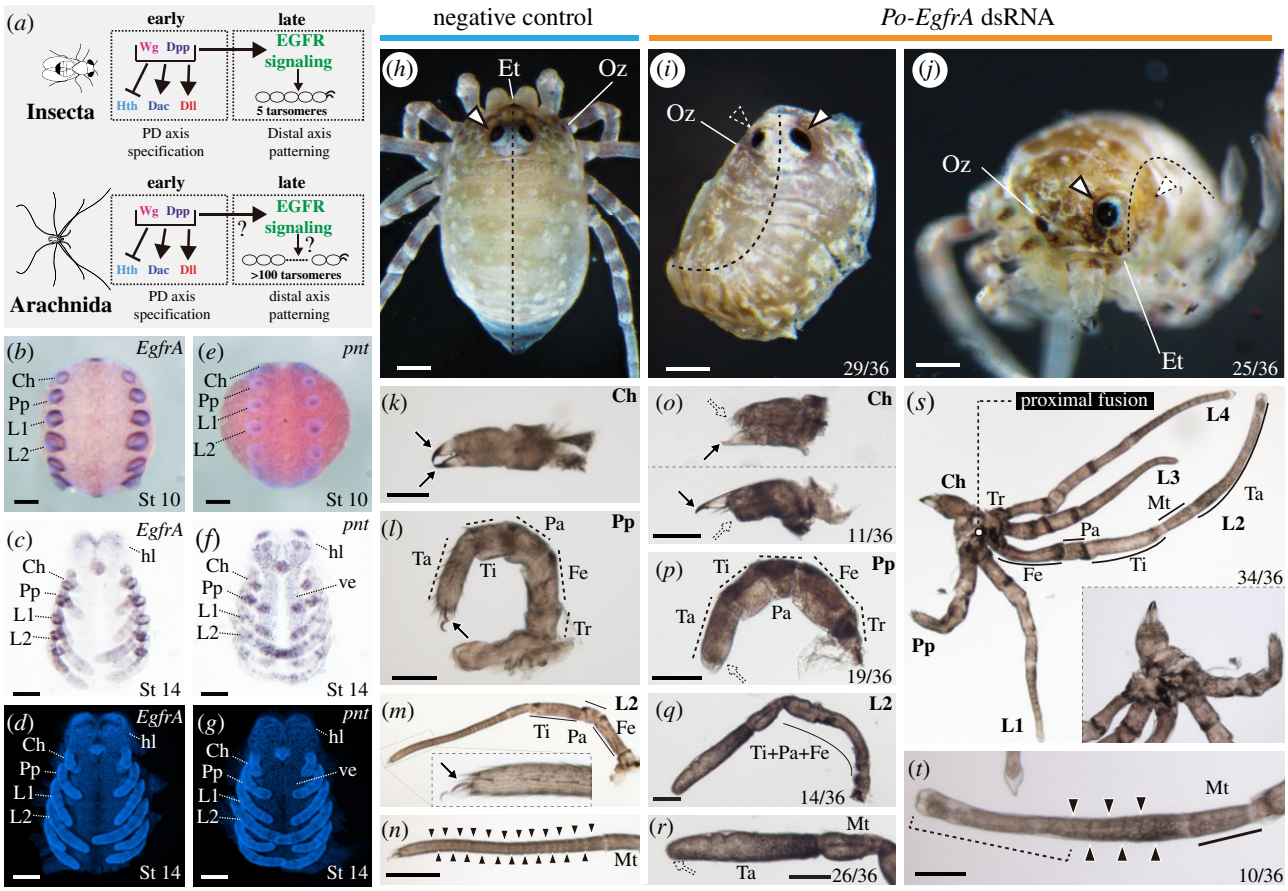

Figure 4. *Po-EgfrA* knockdown affects dorsal patterning, eyes and appendage formation. (*a*) Gene regulatory network specifying PD axis and distal appendage patterning in insects and arachnids. *Po-EgfrA* (*b–d*) and *Po-pnt* (*e–g*) *in situ* hybridization wild-type expression. (*b,e*) Whole-mount stage 10 embryos, merged brightfield and Hoechst nuclear staining, ventral view. (*c,f*) Flatmounts, stage 14 embryos, brightfield, ventral view. (*d,g*) Hoechst nuclear counter staining. (*h*) Negative control hatchling in dorsal view. (*h,j*) Hatchlings from *Po-EgfrA* dsRNA-injected treatment (mosaic, left side affected). (*b*) Hatchling in dorsal view. Note dorsal fusion on the left side of the body ($n = 29/36$). (*c*) Hatchling in frontal view, with the left eye absent. A subset of *Egfr* phenotypes showed eye reduction (25/36) (*k–n*) Appendage flat mounts of negative control hatchlings, in lateral view. (*k*) Chelicera. (*l*) Pedipalp. (*m*) L2. Inset: detail of the claw. (*n*) Tarsus of L2. (*o–t*) Appendage flat mounts of hatchlings of *Po-EgfrA* dsRNA-injected treatment, in lateral view. (*o*) Chelicerae with a reduced fixed finger (upper panel), movable finger (lower panel) or both ($n = 11/36$). (*p*) Pedipalps lacking claw ($n = 19/36$). (*q*) L2, exhibiting podomere fusions proximal to the tarsus ($n = 14/36$). (*r*) Distal end of L2, exhibiting claw and tarsomere reduction ($n = 26/36$). (*s*) Proximal fusion in adjacent appendages (Ch–L4) ($n = 34/36$). Inset: Detail of fused coxae. (*t*) Tarsus of leg 2 shown in (*r*). Weakly affected legs lacked claws and distal tarsal joints (brackets) but retained proximal joints ($n = 10/36$). Arrow, claw; outlined white arrowhead, eye; dotted white arrowhead, eye defect; solid black arrowhead, tarsomere joints; Ch, chelicera; Et, egg tooth; Fe, femur; hl, head lobe; L1–L4, legs 1–4; Mt, metatarsus; Oz, ozophore; Pa, patella; Pp, pedipalp; Ta, tarsus; Ti, tibia; Tr, trochanter; ve, ventral ectoderm. Scale bars: 100 µm. (Online version in colour.)

Nevertheless, the assumed unduplicated condition of the Opiliones genome has not been rigorously tested. The efficiency of developmental transcriptomes in discovering paralogy is a function of sequencing depth and sampling strategy, and thus transcriptomes frequently fail to capture paralogues [1,2,5]. As a first step in validating the use of *P. opilio* as an effective outgroup to Arachnopulmonata, we assembled and interrogated the genome of *P. opilio*, which revealed no evidence of systemic genome duplication events previously reported for arachnopulmonates or horseshoe crabs. Together with the genome architecture of model systems like *I. scapularis* and *T. urticae*, the condition of the harvestman genome strongly supports the inference that an unduplicated genome is the ancestral condition for arachnids.

Having established that Hox genes of *P. opilio* are *bona fide* single-copy, we targeted the first functional datapoints for single-copy Hox genes in any arachnid species, focusing on genes that pattern walking leg identity. We were able to show that the knockdown of *Po-Dfd* affects the identity of legs 1 and 2. This discovery is significant for two reasons. First, two copies of *Dfd* occur in spiders and these exhibit subdivision of expression pattern, with *Ptep-DfdA* being expressed throughout leg tissues and ventral ectoderm, and *Ptep-DfdB* mostly restricted to the ventral ectoderm [4]. It has been shown that the spider paralogue *Ptep-DfdA* is necessary for repressing pedipalp identity on a single-body segment (L1); there is no effect on L2 [38]. Compared to the *Po-Dfd* RNAi phenotype, these data are congruent with the hypothesis that arachnopulmonate *Dfd* paralogues have undergone subfunctionalization. Further functional studies of *DfdB* paralogues in arachnopulmonates are necessary to test this scenario, specifically targeting *DfdB* (alone and also through double knockdown with *DfdA*). Second, segments affected by *Dfd* knockdown in harvestman (L1 and L2) are positionally homologous to those affected by *Dfd* knockdown in pancrustaceans (mandibular and maxillary segments [49–51]). These results bring further support for the notion that the establishment of some Hox anterior boundaries predates the evolution of tagmata, with further substantiation from Hox anterior boundaries in Onychophora [52].

Furthermore, we found that the knockdown of *Po-Scr* alone has no discernible phenotype, whereas the double knockdown of *Po-Dfd* and *Po-Scr* resulted in homeotic transformation of L1–L3 into pedipalps. These data suggest functional redundancy of *Scr* in L3, paralleling the dynamics of *Ubx* and *abdA* in insects; the knockdown of *abdA* alone has a limited effect on homeotic abdominal-to-thoracic segment transformations, whereas the double knockdown of both these genes results in more complete transformations of abdominal segments into thoracic identities [53]. Similar functional redundancy has been shown for *Antp-1* and *Ubx-1* in the spider *P. tepidariorum* [54].

As these experiments show, *P. opilio* has the potential to serve as an informative outgroup to Arachnopulmonata for the study of paralogue divergence after duplication. In addition to newly generated genomic resources, the effectiveness of single and double RNAi in this system makes *P. opilio* an opportune point of comparison for future investigations of arachnid body plan evolution.

(b) A conserved role for epidermal growth factor receptor signalling in appendage patterning across Arthropoda

In the fruit fly *Drosophila melanogaster*, EGFR-Ras signalling is responsible for patterning the legs in two phases. First, EGFR signalling begins with a distal expression (central in the leg disc) of the EGFR ligands in the leg disc [40,41]. The reduction of EGFR signalling results in progressively greater deletion of more distal leg structures, which is consistent with a distal-to-proximal requirement gradient of EGFR signalling by downstream tarsal patterning genes, and with a distal source of EGFR signalling [15,40,41]. A distal source of EGFR signalling is also in accordance with the distal-to-proximal requirement for EGFR signalling in the regenerating leg of the cricket *G. bimaculatus* [45]. In *P. opilio*, 72% ($n = 26/36$) of the hatchlings resulting from RNAi against *Egfr* exhibited defects in the tarsus. These defects ranged from the absence of claws and distal tarsomere fusions, to complete failure to form all tarsal subdivisions. The spectrum of increasingly severe defects from distal-to-proximal observed upon *Egfr* knockdown in *P. opilio* suggests that daddy-long-leg tarsomeres are patterned by a gradient of EGFR signalling similar to *D. melanogaster* and *G. bimaculatus*. This conclusion is further supported by the expression of the EGFR signalling effector *Po-pnt*, which we showed to occur on the tip of the developing appendages at the limb bud stage.

In a second phase, EGFR ligands are expressed as rings at the boundaries of embryonic tarsomeres [39]. The reduction or upregulation of EGFR signalling at this later stage in *D. melanogaster* results in defects in medial tarsomeres and in failure to correctly pattern the tarsal joints [40,41]. However, in short germ insect models (e.g. beetle, water strider and cricket), *Egfr* is expressed as rings at the boundaries of all leg segments proximal to the tarsus, in contrast to rings restricted to the tarsus in the fruit fly [43–45]. RNAi-mediated knockdown in two insect models resulted in leg segment truncations proximal to the tarsus [43,44]. Our data in the arachnid *P. opilio* largely accord with the expression and functional results in short germ insects: 38% ($n = 14/36$) of *Po-EgfrA* RNAi phenotypes also exhibited leg segment fusions proximal to the tarsus. The signal effector *Po-pnt* is also expressed in a distal domain forming rings in later stages of appendage development, which accords with the second phase of expression in model insects [39,43]. Together, these results suggest that the second role of EGFR signalling in leg segmentation may also be conserved in *P. opilio*.

Disentangling the effects of early versus late EGFR signalling phases in the phenotypes observed in *Po-EgfrA* RNAi could be further explored by disrupting EGFR signalling in later development, to surpass the early function in PD axis development. We anticipate that the genome of *P. opilio* will facilitate the development of more sophisticated tools for functional genetics, toward refining the understanding of how daddy-long-legs make their long legs.

Data accessibility. The data underlying this article are available in the article and in its online supplementary material. The genome assembly, EGFR tree and alignment, are available from the Dryad Digital Repository: https://doi.org/10.5061/dryad.ht76hdrds [55]. Sequencing data are deposited in NCBI under accession numbers NCBI PRJNA690950 (RNA-seq), NCBI PRJNA647749 (genome), NCBI SRR12286133 (long reads), NCBI SRR12286133 (short reads). The genome browser is available at: http://phalangium-opilio.sigenomehub.org/.

The data are provided in electronic supplementary material [56].

Authors' contributions. G.G.: conceptualization, data curation, formal analysis, investigation, methodology, validation, visualization, writing-original draft, writing-review and editing; V.L.G.: conceptualization, data curation, formal analysis, funding acquisition, investigation, methodology, software, visualization, writing-original draft, writing-review and editing; J.B.: data curation, formal analysis, methodology, software, writing-review and editing; E.V.W.S.: data curation, methodology, writing-review and editing; C.M.B.: resources, writing-review and editing; L.B.G.: data curation, investigation, writing-review and editing; C.E.S.-L.: data curation, formal analysis, investigation, methodology, writing-review and editing; J.A.C.: funding acquisition, resources, supervision, writing-review and editing; P.S.: conceptualization, data curation, formal analysis, funding acquisition, investigation, methodology, project administration, resources, supervision, validation, writing-original draft, writing-review and editing

All authors gave final approval for publication and agreed to be held accountable for the work performed therein.

Competing interests. We declare we have no competing interests.

Funding. This material is based on work supported by the Food and Drug Administration (J.A.C.), the Global Genome Initiative grant no. GGI-Exploratory-2016-047 (V.L.G.), and National Science Foundation grant nos. IOS-1552610 and IOS-2019141 (P.P.S.). G.G. was supported by a Wisconsin Alumni Research Foundation Fall Research Competition award.

Acknowledgements. RNA sequencing was performed at the Center for Systems Biology, Harvard University. Genomic laboratory work was conducted at the Smithsonian Laboratories of Analytical Biology (LAB). Specimen vouchering and long-term cryogenic curation was provided by the Smithsonian National Museum of Natural History. HCR was made possible by the Patel lab and the 2021 MBL embryology course. Microscopy was performed at the Newcomb Imaging Center, Department of Botany, University of Wisconsin-Madison. Computing was conducted by the Smithsonian Institution High Performance Cluster (https://doi.org/10.25572/SIHPC). Audrey R. Crawford and Calvin So assisted with harvestman rearing and RNAi experiments.

References

1. Sharma PP, Schwager EE, Extavour CG, Wheeler WC. 2014 Hox gene duplications correlate with posterior heteronomy in scorpions. *Proc. R. Soc. B* **281**, 20140661. (doi:10.1098/rspb.2014.0661)
2. Leite DJ *et al*. 2018 Homeobox gene duplication and divergence in arachnids. *Mol. Biol. Evol.* **35**, 2240–2253. (doi:10.1093/molbev/msy125)
3. Leite DJ, Ninova M, Hilbrant M, Arif S, Griffiths-Jones S, Ronshaugen M, McGregor AP. 2016 Pervasive microRNA duplication in chelicerates: insights from the embryonic microRNA repertoire of the spider *Parasteatoda tepidariorum*. *Genome Biol. Evol.* **8**, 2133–2144. (doi:10.1093/gbe/evw143)
4. Schwager EE *et al.* 2017 The house spider genome reveals an ancient whole-genome duplication during arachnid evolution. *BMC Biol.* **15**, 62. (doi:10.1186/s12915-017-0399-x)
5. Ontano AZ *et al.* 2021 Taxonomic sampling and rare genomic changes overcome long-branch attraction in the phylogenetic placement of pseudoscorpions. *Mol. Biol. Evol.* **38**, 2446–2467. (doi:10.1093/molbev/msab038)
6. Nolan ED, Santibáñez López CE, Sharma PP. 2020 Developmental gene expression as a phylogenetic data class: support for the monophyly of Arachnopulmonata. *Dev. Genes Evol.* **230**, 137–153. (doi:10.1007/s00427-019-00644-6)
7. Kenny NJ *et al.* 2015 Ancestral whole-genome duplication in the marine chelicerate horseshoe crabs. *Heredity* **116**, 190–199. (doi:10.1038/hdy.2015.89)
8. Shingate P, Ravi V, Prasad A, Tay BH, Garg KM, Chattopadhyay B, Yap LM, Rheindt FE, Venkatesh B. 2020 Chromosome-level assembly of the horseshoe crab genome provides insights into its genome evolution. *Nat. Commun.* **11**, 1–13. (doi:10.1038/s41467-020-16180-1)
9. Shingate P, Ravi V, Prasad A, Tay BH, Venkatesh B. 2020 Chromosome-level genome assembly of the coastal horseshoe crab (*Tachypleus gigas*). *Mol. Ecol. Resour.* **20**, 1748–1760. (doi:10.1111/1755-0998.13233)
10. Grbić M *et al.* 2011 The genome of *Tetranychus urticae* reveals herbivorous pest adaptations. *Nature* **479**, 487–492. (doi:10.1038/nature10640)
11. Hoy MA *et al.* 2016 Genome sequencing of the phytoseiid predatory mite *Metaseiulus occidentalis* reveals completely atomized Hox genes and superdynamic intron evolution. *Genome Biol. Evol.* **8**, 1762–1775. (doi:10.1093/gbe/evw048)
12. Ballesteros JA, Sharma PP. 2019 A critical appraisal of the placement of Xiphosura (Chelicerata) with account of known sources of phylogenetic error. *Syst. Biol.* **68**, 896–917. (doi:10.1093/sysbio/syz011)
13. Lozano-Fernandez J, Tanner AR, Giacomelli M, Carton R, Vinther J, Edgecombe GD, Pisani D. 2019 Increasing species sampling in chelicerate genomic-scale datasets provides support for monophyly of Acari and Arachnida. *Nat. Commun.* **10**, 2295–2298. (doi:10.1038/s41467-019-10244-7)
14. Sharma PP, Schwager EE, Extavour CG, Giribet G. 2012 Hox gene expression in the harvestman *Phalangium opilio* reveals divergent patterning of the chelicerate opisthosoma. *Evol. Dev.* **14**, 450–463. (doi:10.1111/j.1525-142X.2012.00565.x)
15. Kojima T. 2017 Developmental mechanism of the tarsus in insect legs. *Curr. Opin. Insect. Sci.* **19**, 36–42. (doi:10.1016/j.cois.2016.11.002)
16. Kenning M, Müller CHG, Sombke A. 2017 The ultimate legs of Chilopoda (Myriapoda): a review on their morphological disparity and functional variability. *PeerJ* **5**, e4023–e4036. (doi:10.7717/peerj.4023)
17. Willemart RH, Farine JP, Gnaspini P. 2009 Sensory biology of Phalangida harvestmen (Arachnida, Opiliones): a review, with new morphological data on 18 species. *Acta Zool.* **90**, 209–227. (doi:10.1111/j.1463-6395.2008.00341.x)
18. Koren S, Walenz BP, Berlin K, Miller JR, Bergman NH, Phillippy AM. 2017 Canu: scalable and accurate long-read assembly via adaptive *k*-mer weighting and repeat separation. *Genome Res.* **27**, 722–736. (doi:10.1101/gr.215087.116)
19. Boetzer M, Pirovano W. 2014 SSPACE-LongRead: scaffolding bacterial draft genomes using long read sequence information. *BMC Bioinf.* **15**, 211. (doi:10.1186/1471-2105-15-211)
20. English AC *et al.* 2012 Mind the gap: upgrading genomes with Pacific Biosciences RS long-read sequencing technology. *PLoS ONE* **7**, e47768. (doi:10.1371/journal.pone.0047768)
21. Walker BJ *et al.* 2014 Pilon: an integrated tool for comprehensive microbial variant detection and genome assembly improvement. *PLoS ONE* **9**, e112963. (doi:10.1371/journal.pone.0112963)
22. Guan D, McCarthy SA, Wood J, Howe K, Wang Y, Durbin R. 2020 Identifying and removing haplotypic duplication in primary genome assemblies. *Bioinformatics* **36**, 2896–2898. (doi:10.1093/bioinformatics/btaa025)
23. Smit A, Hubley R, Green P. 2015. *RepeatMasker Open-4.0. 2013*–2015.
24. Hoff KJ, Lomsadze A, Borodovsky M, Stanke M. 2019 Whole-genome annotation with BRAKER. *Methods Mol. Biol.* **1962**, 65–95. (doi:10.1007/978-1-4939-9173-0_5)
25. Hoff KJ. 2019 MakeHub: fully automated generation of UCSC genome browser assembly hubs. *Genom. Proteom. Bioinform.* **17**, 546–549. (doi:10.1016/j.gpb.2019.05.003)
26. Altschul SF, Gish W, Miller W, Myers EW, Lipman DJ. 1990 Basic local alignment search tool. *J. Mol. Biol.* **215**, 403–410. (doi:10.1016/S0022-2836(05)80360-2)
27. Sharma PP, Schwager EE, Giribet G, Jockusch EL, Extavour CG. 2013 *Distal-less* and *dachshund* pattern both plesiomorphic and apomorphic structures in chelicerates: RNA interference in the harvestman *Phalangium opilio* (Opiliones). *Evol. Dev.* **15**, 228–242. (doi:10.1111/ede.12029)
28. Bruce HS, Jerz G, Kelly S, McCarthy J, Pomerantz A, Senevirathne G, Sherrard A, Sun DA, Wolff C, Patel NH. 2021 Hybridization chain reaction (HCR) in situ protocol. (doi:10.17504/protocols.io.bunznvf6)
29. Gulia-Nuss M *et al.* 2016 Genomic insights into the *Ixodes scapularis* tick vector of Lyme disease. *Nat. Commun.* **7**, 10507. (doi:10.1038/ncomms10507)
30. Waterhouse RM, Seppey M, Simão FA, Manni M, Ioannidis P, Klioutchnikov G, Kriventseva EV, Zdobnov EM. 2017 BUSCO applications from quality assessments to gene prediction and phylogenomics. *Mol. Biol. Evol.* **35**, 543–548. (doi:10.1093/molbev/msx319)
31. Chipman AD *et al.* 2014 The first myriapod genome sequence reveals conservative arthropod gene content and genome organisation in the centipede *Strigamia maritima*. *PLOS Biol.* **12**, e1002005. (doi:10.1371/journal.pbio.1002005)
32. Pace RM, Grbić M, Nagy LM. 2016 Composition and genomic organization of arthropod Hox clusters. *EvoDevo* **7**, 1–11. (doi:10.1186/s13227-016-0048-4)
33. Setton EVW, March LE, Nolan ED, Jones TE, Cho H, Wheeler WC, Extavour CG, Sharma PP. 2017 Expression and function of *spineless* orthologs correlate with distal deutocerebral appendage morphology across Arthropoda. *Dev. Biol.* **430**, 224–236. (doi:10.1016/j.ydbio.2017.07.016)
34. Schomburg C, Turetzek N, Schacht MI, Schneider J, Kirfel P, Prpic NM, Posnien N. 2015 Molecular characterization and embryonic origin of the eyes in the common house spider *Parasteatoda tepidariorum*. *EvoDevo* **6**, 15. (doi:10.1186/s13227-015-0011-9)
35. Samadi L, Schmid A, Eriksson BJ. 2015 Differential expression of retinal determination genes in the principal and secondary eyes of *Cupiennius salei* Keyserling (1877). *EvoDevo* **6**, 16. (doi:10.1186/s13227-015-0010-x)
36. Gainett G, Ballesteros JA, Kanzler CR, Zehms JT, Zern JM, Aharon S, Gavish-Regev E, Sharma PP. 2020 Systemic paralogy and function of retinal determination network homologs in arachnids. *BMC Genom.* **21**, 811–817. (doi:10.1186/s12864-020-07149-x)
37. Telford MJ, Thomas RH. 1998 Expression of homeobox genes shows chelicerate arthropods retain their deutocerebral segment. *Proc. Natl Acad. Sci. USA* **95**, 10 671–10 675. (doi:10.1073/pnas.95.18.10671)
38. Pechmann M, Schwager EE, Turetzek N, Prpic NM. 2015 Regressive evolution of the arthropod tritocerebral segment linked to functional divergence of the Hox gene *labial*. *Proc. R. Soc. B* **282**, 20151162. (doi:10.1098/rspb.2015.1162)
39. Galindo MI, Bishop SA, Couso JP. 2005 Dynamic EGFR-Ras signalling in *Drosophila* leg development.

Dev. Dyn. **233**, 1496–1508. (doi:10.1002/dvdy.20452)

40. Campbell G. 2002 Distalization of the *Drosophila* leg by graded EGF-receptor activity. *Nature* **418**, 781–785. (doi:10.1038/nature00971)
41. Galindo MI, Bishop SA, Greig S, Couso JP. 2002 Leg patterning driven by proximal–distal interactions and EGFR signaling. *Science* **297**, 256–259. (doi:10.1126/science.1072311)
42. Brunner D, Dücker K, Oellers N, Hafen E, Scholzi H, Klämbt C. 1994 The ETS domain protein Pointed-P2 is a target of MAP kinase in the Sevenless signal transduction pathway. *Nature* **370**, 386–389. (doi:10.1038/370386a0)
43. Grossmann D, Prpic NM. 2012 Egfr signaling regulates distal as well as medial fate in the embryonic leg of *Tribolium castaneum*. *Dev. Biol.* **370**, 264–272. (doi:10.1016/j.ydbio.2012.08.005)
44. Refki PN, Khila A. 2015 Key patterning genes contribute to leg elongation in water striders. *EvoDevo* **6**, 14. (doi:10.1186/s13227-015-0015-5)
45. Nakamura T, Mito T, Miyawaki K, Ohuchi H, Noji S. 2008 EGFR signaling is required for re-establishing the proximodistal axis during distal leg regeneration in the cricket *Gryllus bimaculatus* nymph. *Dev. Biol.* **319**, 46–55. (doi:10.1016/j.ydbio.2008.04.002)
46. Halfar K, Rommel C, Stocker H, Hafen E. 2001 Ras controls growth, survival and differentiation in the *Drosophila* eye by different thresholds of MAP kinase activity. *Development* **128**, 1687–1696. (doi:10.5167/uzh-625)
47. Gainett G, Sharma PP. 2020 Genomic resources and toolkits for developmental study of whip spiders (Amblypygi) provide insights into arachnid genome evolution and antenniform leg patterning. *EvoDevo* **11**, 18–18. (doi:10.1186/s13227-020-00163-w)
48. Baudouin-Gonzalez L *et al.* 2021 The evolution of Sox gene repertoires and regulation of segmentation in arachnids. *Mol. Biol. Evol.* msab088. (doi:10.1093/molbev/msab088)
49. Brown S, DeCamillis M, Gonzalez-Charneco K, Denell M, Beeman R, Nie W, Denell R. 2000 Implications of the *Tribolium Deformed* mutant phenotype for the evolution of Hox gene function. *Proc. Natl Acad. Sci. USA* **97**, 4510–4514. (doi:10.1073/pnas.97.9.4510)
50. Hughes CL, Kaufman TC. 2000 RNAi analysis of Deformed, proboscipedia and Sex combs reduced in the milkweed bug *Oncopeltus fasciatus*: novel roles for Hox genes in the hemipteran head. *Development* **127**, 3683–3694. (doi:10.1242/dev.127.17.3683)
51. Martin A, Serano JM, Jarvis E, Bruce HS, Wang J, Ray S, Barker CA, O'Connell LC, Patel NH. 2016 CRISPR/Cas9 mutagenesis reveals versatile roles of Hox genes in crustacean limb specification and evolution. *Curr. Biol.* **26**, 14–26. (doi:10.1016/j.cub.2015.11.021)
52. Janssen R, Eriksson BJ, Tait NN, Budd GE. 2014 Onychophoran Hox genes and the evolution of arthropod Hox gene expression. *Front. Zool.* **11**, 22. (doi:10.1186/1742-9994-11-22)
53. Angelini DR, Liu PZ, Hughes CL, Kaufman TC. 2005 Hox gene function and interaction in the milkweed bug *Oncopeltus fasciatus* (Hemiptera). *Dev. Biol.* **287**, 440–455. (doi:10.1016/j.ydbio.2005.08.010)
54. Khadjeh S, Turetzek N, Pechmann M, Schwager EE, Wimmer EA, Damen WGM, Prpic NM. 2012 Divergent role of the Hox gene *Antennapedia* in spiders is responsible for the convergent evolution of abdominal limb repression. *Proc. Natl Acad. Sci. USA* **109**, 4921–4926. (doi:10.1073/pnas.1116421109)
55. Gainett G, González VL, Ballesteros JA, Setton EVW, Baker CM, Barolo Gargiulo L, Santibáñez-López CE, Coddington JA, Sharma PP. 2021 Data from: The genome of a daddy-long-legs (Opiliones) illuminates the evolution of arachnid appendages. Dryad Digital Repository. (https://doi.org/10.5061/dryad.ht76hdrds)
56. Gainett G, González VL, Ballesteros JA, Setton EVW, Baker CM, Barolo Gargiulo L, Santibáñez-López CE, Coddington JA, Sharma PP. 2021 Data from: The genome of a daddy-long-legs (Opiliones) illuminates the evolution of arachnid appendages. Figshare.